International Journal of Nanomedicine

Dovepress
open access to scientific and medical research

Open Access Full Text Article

ORIGINAL RESEARCH

Combined Chemo- and Photothermal Therapies of Non-Small Cell Lung Cancer Using Polydopamine/Au Hollow Nanospheres Loaded with Doxorubicin

Xinbo Zhang, Bin Xu, Jiangwei Ni, Yucheng Xiang, Zhifeng He

Department of Thoracic Surgery, The First Affiliated Hospital of Wenzhou Medical University, Wenzhou, Zhejiang, People's Republic of China

Correspondence: Zhifeng He, Department of Thoracic Surgery, The First Affiliated Hospital of Wenzhou Medical University, Wenzhou, Zhejiang, People's Republic of China, Email hezhifeng@wzhospital.cn

Purpose: The chemotherapeutic agent doxorubicin (DOX) is limited by its cardiotoxicity, posing challenges in its application for non-small cell lung cancer (NSCLC). This study aims to explore the efficacy of polydopamine/Au nanoparticles loaded with DOX for chemotherapy and photothermal therapy in NSCLC to achieve enhanced efficacy and reduced toxicity.

Methods: Hollow polydopamine (HPDA)/Au@DOX was synthesized via polydopamine chemical binding sacrificial template method. Morphology was characterized using transmission electron microscopy, particle size and potential were determined using dynamic light scattering, and photothermal conversion efficiency was assessed using near-infrared (NIR) thermal imaging. Drug loading rate and in vitro drug release were investigated. In vitro, anti-tumor experiments were conducted using CCK-8 assay, flow cytometry, and live/dead cell staining to evaluate the cytotoxicity of HPDA/Au@DOX on A549 cells. Uptake of HPDA/Au@DOX by A549 cells was detected using the intrinsic fluorescence of DOX. The in vivo anti-metastasis and anti-tumor effects of HPDA/Au@DOX were explored in mouse lung metastasis and subcutaneous tumor models, respectively.

Results: HPDA/Au@DOX with a particle size of (164.26±3.25) nm, a drug loading rate of 36.31%, and an encapsulation efficiency of 90.78% was successfully prepared. Under 808 nm laser irradiation, HPDA/Au@DOX accelerated DOX release and enhanced uptake by A549 cells. In vitro photothermal performance assessment showed excellent photothermal conversion capability and stability of HPDA/Au@DOX under NIR laser irradiation. Both in vitro and in vivo experiments demonstrated that the photothermal-chemotherapy combination group (HPDA/Au@DOX+NIR) exhibited stronger anti-metastatic and anti-tumor activities compared to the monotherapy group (DOX).

Conclusion: HPDA/Au@DOX nanosystem demonstrated excellent photothermal effect, inhibiting the growth and metastasis of A549 cells. This nanosystem achieves the combined effect of chemotherapy and photothermal, making it promising for NSCLC treatment.

Keywords: non-small cell lung cancer, chemotherapy, photothermal therapy, doxorubicin, Au nanoparticles

Introduction

Lung cancer is one of the most common and deadliest cancers worldwide, with over 2.2 million new cases reported annually and approximately 1.79 million deaths.[1] In China, lung cancer remains the cancer with the highest incidence and mortality rates, with around 730,000 new cases diagnosed and 610,000 deaths attributed to lung cancer each year.[2] Due to limitations in early lung cancer screening techniques, the majority of lung cancer patients are diagnosed at an advanced stage, necessitating chemotherapy or radiotherapy for life extension and improvement of quality of life.[3] Lung cancer is divided into non-small cell lung cancer (NSCLC) and small cell lung cancer (SCLC), with NSCLC accounting for approximately 80%-85% of all lung cancer cases and imposing significant economic and social burdens.[4] As one of the most effective and widely used anticancer drugs, despite continuous iterations of anticancer drugs, doxorubicin (DOX) is still extensively employed in various lung cancer

Received: 18 June 2024
Accepted: 10 September 2024
Published: 14 September 2024

Graphical Abstract

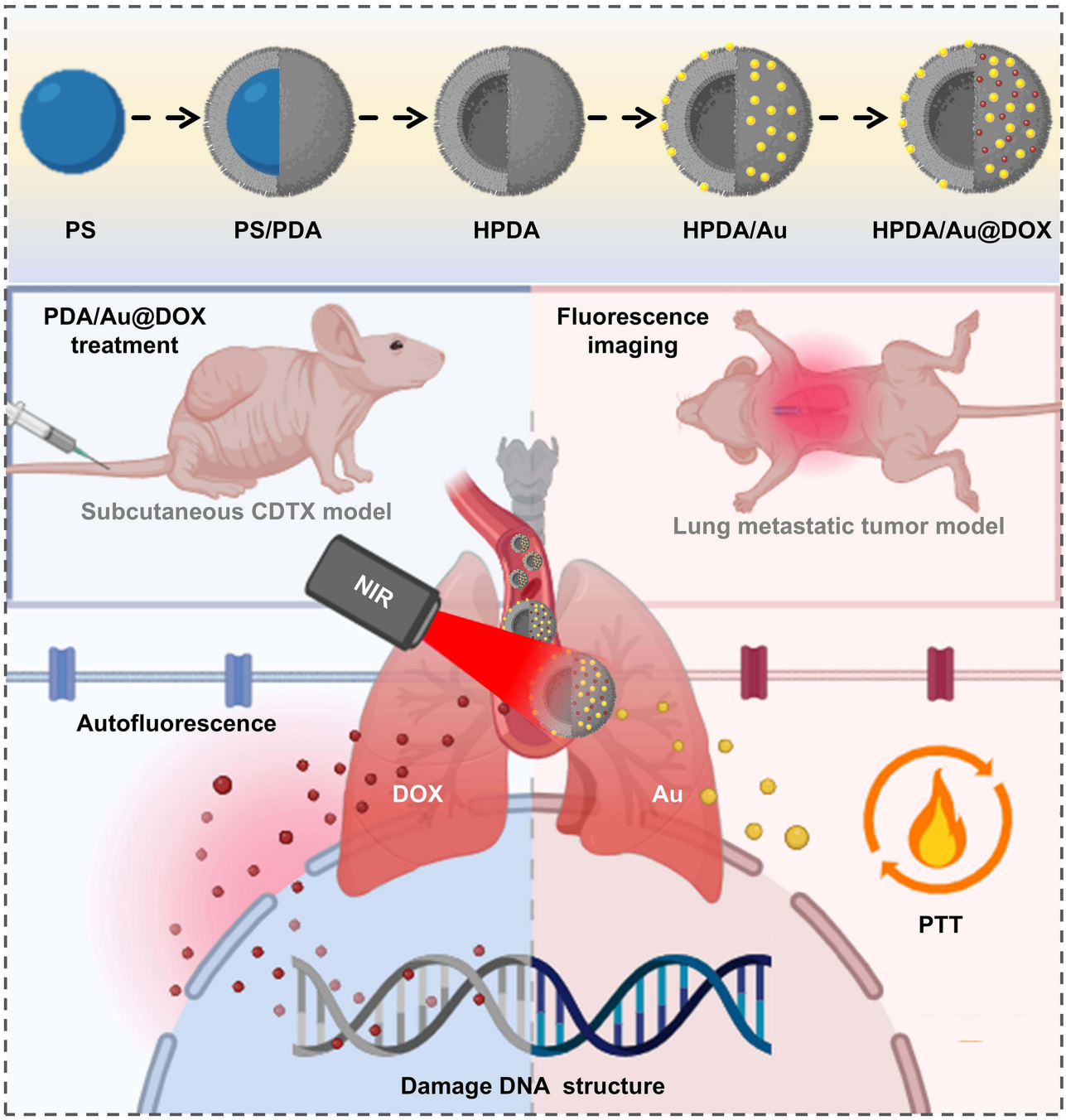

treatment regimens.[5–7] Unfortunately, the cardiotoxicity and myelosuppression induced by DOX are significant limiting factors in clinical applications.[8,9] The incidence of clinical heart failure during DOX chemotherapy increases dose-dependently, with a heart failure rate of 48% when the cumulative dose reaches 700 mg/m².[10] Therefore, finding a drug delivery method that can enhance the efficacy of DOX while reducing systemic toxic side effects is particularly important.

In recent years, nanocarriers have been widely employed in the field of controlled drug release for cancer therapy.[11,12] Nanocarriers can deliver drugs to targets, achieving precise control over drug release in both time and space, thereby enhancing efficacy while reducing toxicity.[13–16] Moreover, through modification and functionalization of nanomaterials, certain nanomaterials themselves can also achieve therapeutic effects on tumors.[17] For instance, photothermal therapy (PTT) mediated by photosensitive nanomaterials can convert near-infrared (NIR) light into thermal energy, leading to tumor ablation. PTT offers advantages such as non-invasiveness, localized action, and minimal side effects, and its efficacy has been widely recognized.[18,19] Traditional clinical hyperthermia involves local heating through heat infusion or infrared light irradiation, but its effect is limited to the surface of tumors and tissues.[20] In recent years, numerous studies have shown that combining PTT with chemotherapy effectively suppresses tumor growth and significantly reduces the toxic side effects of chemotherapy.[21–23] Nanomaterials can maintain high concentrations of therapeutic drugs in the bloodstream while prolonging their circulation time in the blood and promoting their penetration into tumors, ultimately enhancing the therapeutic effect of PTT on deep-seated tumors.[24]

Polydopamine (PDA) is synthesized through oxidative polymerization of dopamine, structurally resembling adhesive proteins secreted by mussels, with excellent biocompatibility and degradability.[25] Additionally, PDA's chemical structure integrates numerous functional groups such as catechol, amino, and imino, endowing it with the ability to construct a variety of composite materials, thus widely applied in the biomedical field.[26] As a drug carrier, PDA is rich in aromatic rings, allowing it to stably load antitumor drugs containing aromatic frameworks, such as DOX, paclitaxel, camptothecin, and curcumin, through π-π stacking interactions under physiological conditions.[27] Furthermore, PDA exhibits good photothermal conversion efficiency, particularly when compared to solid PDA nanoparticles of the same size and concentration, with hollow PDA nanoparticles showing higher photothermal conversion efficiency (40.4% vs 37.1%).[28]

Meanwhile, Gold nanoparticles (AuNPs) exhibit strong surface plasmon resonance (SPR) in the near-infrared region, effectively converting absorbed NIR light into heat, making them ideal candidates for PTT.[29] Due to their excellent biocompatibility and remarkable photophysical properties, AuNPs have broad application prospects in biomedicine, including photothermal ablation of cancer cells, drug delivery, and photoacoustic imaging.[30–34] The introduction of AuNPs provides the possibility of integrating molecular imaging with tumor therapy, facilitating the exploration of integrated diagnosis and treatment of NSCLC. In recent years, PDA hollow nanospheres modified with AuNPs have garnered increasing attention due to their immense potential in PTT applications.[35] Combining these with chemotherapeutic drugs like DOX holds promise in mitigating the side effects of DOX while addressing the challenge of heat shock protein overexpression, which may lead to tumor resistance to hyperthermia during prolonged use of single PTT.[36]

Therefore, this study designed a PDA hollow sphere with surface-modified AuNPs as a carrier, and after loading DOX into it, HPDA/Au@DOX was formed to explore the inhibitory effect of HPDA/Au@DOX combined with PTT on NSCLC A549 cells. This structure was designed to make full use of the cytotoxicity of chemotherapeutic drugs as well as the photothermal conversion properties of PDA and AuNPs to achieve a double blow against tumors. First, the characterization, photothermal properties, and drug release behavior of HPDA/Au@DOX were investigated. Second, its good uptake and anti-tumor activity in A549 cells were verified by in vitro cellular experiments. In vivo experiments were used to further evaluate the biocompatibility, anti-metastatic, and anti-tumor effects of HPDA/Au@DOX.

Methods

Materials

Dopamine, Tris-HCl buffer solution, polystyrene (PS), ethanol, trichloromethane, DOX, and $HAuCl_4$ were purchased from Aladdin (Shanghai, China). Cell Counting Kit-8 (CCK-8, C0037), Annexin V-FITC Apoptosis Detection Kit (C1062S), and Calcein/PI Cell Activity and Cytotoxicity Assay Kit (C2015S) were purchased from Beyotime Biotechnology (Shanghai, China).

Preparation of HPDA/Au@DOX

Firstly, dopamine (200 mg) was dissolved in a freshly prepared Tris-HCl buffer solution (100 mL, 10 mM, pH 8.5) to prepare a dopamine solution (2 mg/mL). Then, PS (0.2 g) was dispersed into the dopamine solution with the assistance of ultrasound. After stirring at room temperature for 24 hours, PDA shells were coated on the PS colloidal spheres. The PS/PDA core-shell composite spheres were separated by centrifugation and washed several times with ethanol. These PS/PDA composite spheres were treated with chloroform to remove the PS template. Hollow PDAs (HPDA) were collected by centrifugation and washed twice with chloroform and ethanol. Then, a solution of $HAuCl_4$ (10 mg/mL) was added to a 30 mL water solution containing 0.1 wt% HPDA. The reaction was stirred at room temperature for 1 hour, and PDA/Au composite spheres were collected by centrifugation and washed several times with ultrapure water and ethanol. PDA/Au was added to a solution of DOX (1 mg/mL), and after stirring at room temperature for 24 hours, the mixture was centrifuged and washed with deionized water to obtain HPDA/Au@DOX.

Characterization of HPDA/Au@DOX

The surface morphology and internal structure of the materials were observed using transmission electron microscopy (TEM, Hitachi, Japan). The hydrated particle size and zeta potential of the materials were measured using a Zetasizer Nano (Zetasizer Nano ZS ZEN3600, Malvern, United Kingdom). After 1, 2, 3, 4, 5, 6, and 7 days of static incubation, dynamic light scattering (DLS) was used again to monitor size changes to evaluate the stability of HPDA/Au@DOX. X-ray powder diffraction (XRD) characterization of the materials was performed using an X-ray diffractometer (Bruker, Germany). UV-visible-near-NIR absorption spectra were recorded using a Shimadzu UV3600 UV-visible-NIR spectrophotometer (Shimadzu Corporation, Japan).

In vitro Photothermal Studies

Firstly, an 808 nm laser (1 W/cm²) was used to irradiate PBS, HPDA, DOX, AuNPs, and a 50 μg/mL HPDA/Au@DOX solution for 10 minutes. The real-time temperature was measured and recorded every 30 seconds using an infrared thermal imager (Fluke, America). Next, the effect of HPDA/Au@DOX solution concentration (0, 6.25, 12.5, 25, 50, 100 μg/mL) and laser power density (0.2, 0.4, 0.6, 0.8, 1.0, 1.2 W/cm²) on photothermal behavior was investigated. To assess the photothermal stability of HPDA/Au@DOX, a 50 μg/mL HPDA/Au@DOX solution was exposed to 808 nm laser (1 W/cm²) irradiation for 10 minutes, followed by natural cooling for 10 minutes, repeated 5 times. Heating-cooling curves were plotted, and photothermal conversion efficiency was calculated.

DOX Loading and Release Behavior

The loading rate of DOX was determined by the UV absorbance (485 nm) of the standard curve, and the loading rate was calculated as: loading rate = m (loaded DOX) / m (Total HPDA/Au@DOX) × 100%. The in vitro DOX release behavior of HPDA/Au@DOX was evaluated with and without NIR laser irradiation conditions. Briefly, a dispersion of 1 mg/mL HPDA/Au@DOX was prepared by adding HPDA/Au@DOX to a PBS solution and sonicated. Then 1 mL of the dispersion was placed in a dialysis bag (molecular weight cut-off = 14,000), which was immersed in a solution containing 10 mL of PBS and continuously shaken (300 r/min) at room temperature. During this period, 1 mL of the solution was removed for analysis at 2, 5, 10, 20, 40, 60, 80, 100, 120, and 240 min, and then an equal volume of PBS buffer was added back in and shaking continued. The DOX content of the corresponding absorbance in each sample was determined and the drug release curve was plotted.

Cell Culture

A549 cells were purchased from iCell Bioscience Inc (Shanghai, China). The cells were cultured in DMEM medium supplemented with 10% fetal bovine serum (FBS) and 1% penicillin-streptomycin. Cell cultures were maintained at 37°C in a humidified atmosphere containing 5% CO_2. Based on the photothermal properties

results, the safe and effective concentration of HPDA/Au@DOX for subsequent experiments was selected through a CCK-8 toxicity assay. In brief, A549 cells were seeded in culture medium containing different concentrations (6.25, 12.5, 25, 50, 100 μg/mL) of HPDA/Au@DOX for 4 hours. NIR laser irradiation was applied to the A549 cells for 5 minutes, followed by further incubation for 44 hours. Subsequently, the cells were incubated with CCK-8 reagent for 3 hours, and cell viability was determined using a microplate reader.

In vitro Anti-Tumor Studies

A549 cells were divided into 5 groups: PBS, PBS+NIR, DOX, HPDA/Au@DOX, and HPDA/Au@DOX+NIR groups. Cells were cultured in fresh medium containing PBS, DOX, and HPDA/Au@DOX, respectively, for 48 hours. If NIR laser irradiation was involved, A549 cells were irradiated for 10 minutes after 4 hours of incubation, followed by further incubation for 44 hours. Cell proliferation was detected using the CCK-8 assay, with the PBS group set as the negative control and cell viability normalized to 100%. Additionally, according to the manufacturer's instructions, flow cytometry and live/dead cell staining were performed using the Annexin V-FITC Cell Apoptosis Detection Kit (C1062S) and the Calcein/PI Cell Viability and Cytotoxicity Detection Kit (C2015S), respectively. The cell seeding, incubation regimen, and drug concentrations were consistent with those used in the CCK-8 assay.

Cellular Uptake

To study the uptake of HPDA/Au@DOX, the intrinsic fluorescence property of DOX was utilized. The cell seeding, drug concentration, and incubation regimen were the same as in the in vitro anti-tumor experiment. After removing the culture medium, cells were washed three times with PBS, fixed with 4% paraformaldehyde for 10 minutes, and then washed three times with PBS. Nucleic acid dye DAPI was incubated with the cells for 20 minutes, the excess dye was washed away with PBS, and the cells were observed under a laser confocal microscope (excitation wavelength: 480 nm, emission wavelength: 590 nm).

Animals

Male 6–8 weeks BALB/c nude mice were provided by SPF Biotechnology Co.,Ltd. (Beijing, China) for the study of the in vivo biosafety, anti-metastasis, and anti-tumor effects of HPDA/Au@DOX. All animal experiments were conducted in accordance with the requirements of the Animal Experiment Ethics Committee of Wenzhou Medical University (Approval No. wydw2024-0156). The nude mice were raised in specific pathogen-free environments, with environmental temperature maintained at 18~22 °C and relative humidity between 40% and 70%.

Hemolysis

Fresh blood (1 mL) from nude mice was centrifuged at 1200 rpm for 10 minutes to separate blood cells. The pellet was washed with PBS until the supernatant became clear, with the pellet representing blood cells. Distilled water was used as the positive control, and PBS served as the negative control. In 0.8 mL of PBS solution containing different concentrations (12.5, 25, 50, 100, 200 μg/mL) of HPDA/Au@DOX, 0.2 mL of blood cells was added and incubated for 2 hours. The samples were then centrifuged at high speed, and the absorbance (A) of the supernatant was measured at a wavelength of 540 nm. The hemolysis rate of the samples was calculated according to the formula.

$$\text{Hemolysis}(\%)=\left(A_{\text{Sample}}-A_{\text{PBS}}\right)/\left(A_{\text{H2O}}-A_{\text{PBS}}\right)\times 100\%$$

Biological Safety Assessment

Male BALB/c nude mice were randomly divided into two groups (n=5): PBS group and HPDA/Au@DOX group. In the HPDA/Au@DOX group, 100 μL of HPDA/Au@DOX (5 mg/kg for DOX) was injected each time, while an equal volume of PBS was injected into the PBS group. Intratracheal injection was administered once every 7 days, totaling 2 doses. Specifically, mice were anesthetized and placed in a supine position on the surgical table with their forelimbs extended and fixed. A small incision of 5~7 mm was made in the neck using surgical

scissors. Holding the trachea with forceps, the injector with the needle angled upward at 45° to the trachea was inserted slowly, and the drug was injected slowly into the trachea. After waiting for 5 s, the needle was slowly withdrawn. The incision was sutured, and the mice were returned to their cages to recover until fully awake. Laser irradiation was performed on the tumor area 12 h after each injection. On the 15th day, the mice were sacrificed, and major organs (heart, liver, spleen, lungs, kidneys) and blood were collected for hematoxylin and eosin (H&E) staining and blood routine and liver and kidney function analysis, respectively, to observe acute toxicity reactions in mice within 15 days.

In vivo Anti-Metastatic Studies

To establish the A549 lung metastasis model, A549 cell suspension (1×10^6 cells) was injected into the tail vein of BALB/c nude mice. One day later, the mice were randomly divided into 5 groups (n=5): PBS, PBS+NIR, DOX, HPDA/Au@DOX, and HPDA/Au@DOX+NIR. In the DOX group and HPDA/Au@DOX group, 100 μL of HPDA/Au@DOX (5 mg/kg for DOX) was injected each time, while an equal volume of PBS was injected into the PBS group. Intratracheal administration was performed once every 7 days for a total of 14 days. Laser irradiation was conducted on the chest area where the lung tumors are located, 12 h after each injection. After the completion of drug administration, lung tissues were excised, photographed, and subjected to H&E staining.

In vivo Fluorescence Imaging

The mice were anesthetized, and images were captured at different time points (0, 1, 3, 6, 9, 12, and 24 hours) following the injection of HPDA/Au@DOX. After live imaging, the mice were immediately euthanized, and major organs (heart, lungs, liver, kidneys, spleen) were harvested for ex vivo imaging.

In vivo Anti-Tumor Study

Subcutaneous injection of A549 cells (2×10^6 cells) was performed near the axilla on the right dorsum of the mice to establish the A549 xenograft nude mouse model. Ten days later, the mice were randomly divided into 6 groups (n=5) for in vivo anti-metastasis research to observe the anti-tumor efficacy of HPDA/Au@DOX. In the DOX group and HPDA/Au@DOX group, 100 μL of HPDA/Au@DOX (5 mg/kg for DOX) was injected each time, while an equal volume of PBS was injected into the PBS group. The intratracheal administration was performed once every 7 days for a total of 21 days. Laser irradiation was conducted on the tumor area for 10 minutes 12 hours after each injection. The temperature values were recorded every 1 minute using a thermal imager (FOTRIC 220, Fei Zhi Ke Intelligent Technology, Shanghai, China), and infrared images were captured to plot the temperature rise curve of the tumor site within 10 minutes. During the treatment process, the body weight of the nude mice and the length and width of the tumors were measured every 2 days using an electronic balance and a vernier caliper, respectively, to calculate the tumor volume. At the end of the treatment, the mice were sacrificed, tumors were excised, and their weights were measured.

Statistical Analysis

Statistical analysis of experimental results was performed using GraphPad Prism 8.0 software. The normality of data distribution was assessed using the Shapiro–Wilk test. Data are presented as mean ± standard deviation (x ± s). The differences between the two groups were analyzed using the *t*-test, while differences among multiple groups were analyzed using one-way analysis of variance (ANOVA). After ANOVA, post hoc analysis was performed by Tukey's test. For DOX release, two-way ANOVA with Sidak's multiple comparisons test was used. For blood biochemical indices at different time points, conformity to normal distribution was analyzed by repeated measures ANOVA, and non-conformity to normal distribution was analyzed by Friedman test. A p-value less than 0.05 was considered statistically significant.

Results and Discussion

Preparation and Characterization of HPDA/Au@DOX

We characterized the surface morphology and internal structure of the materials using TEM (Figure 1A). Following the removal of the PS template from the core-shell structured PS/PDA composite spheres, HPDA was obtained with a spherical morphology and an average diameter of approximately 150 nm. HPDA, acting as a reducing agent, facilitated the in situ reduction of $AuCl_4^-$ ions to metallic AuNPs under mild conditions, resulting in a uniform distribution of AuNPs on the HPDA surface. DOX was then loaded into HPDA/Au through physical adsorption, ultimately synthesizing HPDA/Au@DOX. Hydrated states of HPDA and HPDA/Au@DOX are depicted in Figure 1B, showing well-dispersed nanosuspensions. DLS measurements supported TEM results, with average sizes of 164.11±3.48 nm for HPDA and 164.26±3.25 nm for HPDA/Au@DOX (Figure 1C and D). Nanomaterials of this size can passively target tumor tissues through the enhanced permeability and retention effect (EPR), potentially increasing therapeutic efficacy and reducing adverse drug reactions.[37] Additionally, the abundant amino groups on PDA surfaces promote interaction with cell membrane

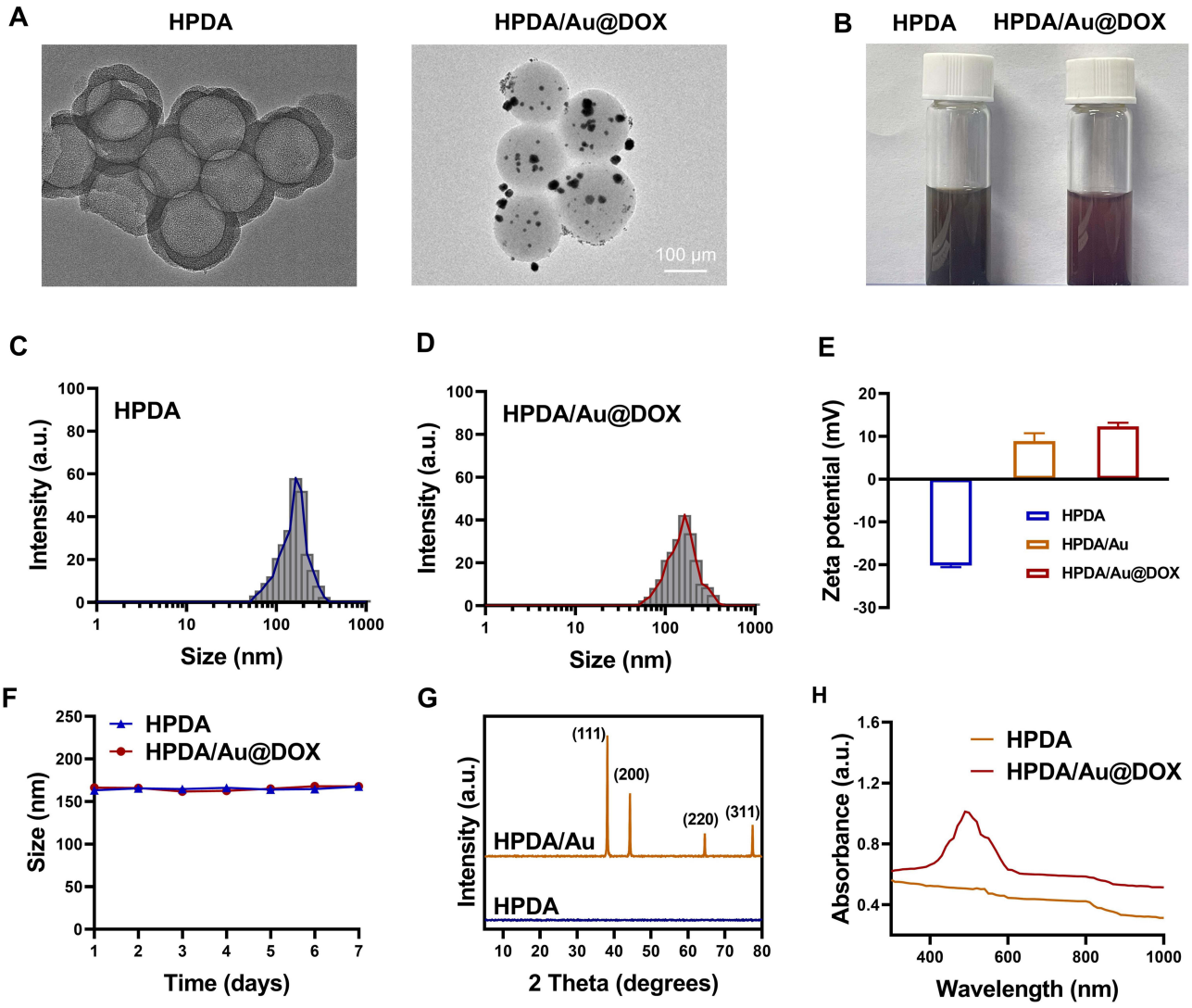

Figure 1 (**A**) Transmission electron microscope images of HPDA and HPDA/Au@DOX (scale bar, 200 nm). (**B**) Hydration states of HPDA and HPDA/Au@DOX. (**C** and **D**) Size distributions of HPDA (**C**) and HPDA/Au@DOX (**D**). (**E**) Surface zeta potentials of HPDA, HPDA/Au, and HPDA/Au@DOX. (**F**) Average particle sizes of HPDA and HPDA/Au@DOX dispersed in water over seven consecutive days. (**G**) X-ray diffraction patterns of PDA and PDA/Au. (**H**) UV-visible-near infrared absorption spectra of PDA and HPDA/Au@DOX in aqueous solution.

proteins, enhancing transmembrane transport and DOX release inside cells, thereby improving chemotherapy effectiveness.[38]

It has shown that positively charged nanoparticles can adhere to the surface of negatively charged tumor cells through electrostatic forces, facilitating the uptake of nanoparticles by tumor cells.[39] HPDA exhibited an average zeta potential of −20.19±0.39 mV, which shifted to positive values for HPDA/Au (8.92±1.82 mV) and HPDA/Au@DOX (12.31±0.87 mV) after AuNPs modification (Figure 1E). HPDA and HPDA/Au@DOX were dispersed in water for 7 days to obtain a stable particle size distribution curve (Figure 1F). After AuNPs modification, XRD showed new peaks at 38.18°, 44.30°, 64.56°, and 77.50°, corresponding to the reflections of the (111), (200), (220), and (311) crystal planes of face-centered cubic (fcc) structured Au (Figure 1G), demonstrating the successful preparation of HPDA/Au. From the UV-visible-infrared absorption spectrum (Figure 1H), the characteristic peak of DOX appeared near 490 nm in HPDA/Au@DOX, indicating successful loading of DOX. Additionally, compared to HPDA, HPDA/Au@DOX showed enhanced absorbance in the long-wavelength region (600–1000 nanometers), suggesting its potential application in the PTT field.

Photothermal Performance and Drug Release Behavior of HPDA/Au@DOX

To validate the photothermal properties of HPDA/Au@DOX, real-time temperatures during laser irradiation (808 nm, 1.0 W/cm^2) for 10 minutes were monitored using an infrared thermal imaging system (Figure 2A). As shown in Figure 2B, the temperature of HPDA/Au@DOX rapidly increased from 26.9°C to 55.2°C under laser irradiation and reached equilibrium after 8 minutes. After irradiation for 10 minutes, the temperatures of AuNPs and HPDA/Au@DOX reached 45.8°C and 55.9°C, respectively. We further investigated the relationship between the concentration of HPDA/Au@DOX and laser power density with photothermal behavior. Under 808 nm irradiation, the temperature increase was significantly correlated with HPDA/Au@DOX concentration and laser power density, with higher concentrations or laser densities resulting in greater temperature increases (Figure 2C and D).

Furthermore, little significant weakening was detected during five consecutive laser on/off cycles (Figure 2E). After turning off the photothermal switch following 10 minutes of laser irradiation, HPDA/Au@DOX quickly returned to room temperature, and consistent temperatures were achieved in subsequent cycles, indicating high photothermal stability. The photothermal conversion efficiency (η) of HPDA/Au@DOX was calculated as 49.3% (Figure 2F), comparable to other DOX-loaded nanomaterials used in PTT.[40–42] The drug loading rate of HPDA/Au@DOX was 36.31% with an encapsulation efficiency of 90.78%. The effect of photothermal conditions on drug release was assessed, revealing a 28% release of DOX without NIR irradiation, which increased to 62% with NIR laser irradiation (Figure 2G). These findings reliably demonstrate that HPDA/Au@DOX effectively releases DOX in response to NIR light and serves as an efficient photothermal conversion material.

In vitro Antitumor Effects of HPDA/Au@DOX

We further investigated the in vitro anti-tumor effect of HPDA/Au@DOX under NIR laser irradiation. CCK-8 assays showed that under NIR laser irradiation, HPDA/Au@DOX exhibited enhanced inhibition of A549 cell viability with increasing concentrations (Figure 3A). However, high concentrations, such as 100 μg/mL, caused temperatures exceeding 60°C, posing risks to normal tissues.[20] Consequently, 50 μg/mL was chosen as the optimal concentration for subsequent experiments due to its balance between efficacy and safety. Further assessments of HPDA/Au@DOX's effects on A549 cell proliferation and apoptosis using CCK-8 and flow cytometry demonstrated that HPDA/Au@DOX+NIR showed the highest toxicity, combining PTT and chemotherapy (Figure 3B–D). As shown in Figure 3E, Calcein-AM/PI dual staining confirmed these findings, showing fewer live cells (green fluorescence, Calcein-AM stained live cells) and more dead cells (red fluorescence, PI stained dead cells). These results indicate that HPDA/Au@DOX exhibits significant anti-tumor activity under NIR laser irradiation.

Uptake by target cells is a fundamental prerequisite for various biomaterials to achieve effective treatment.[43] Based on the intrinsic fluorescence of DOX, cellular uptake of HPDA/Au@DOX in A549 cells was tracked using fluorescence

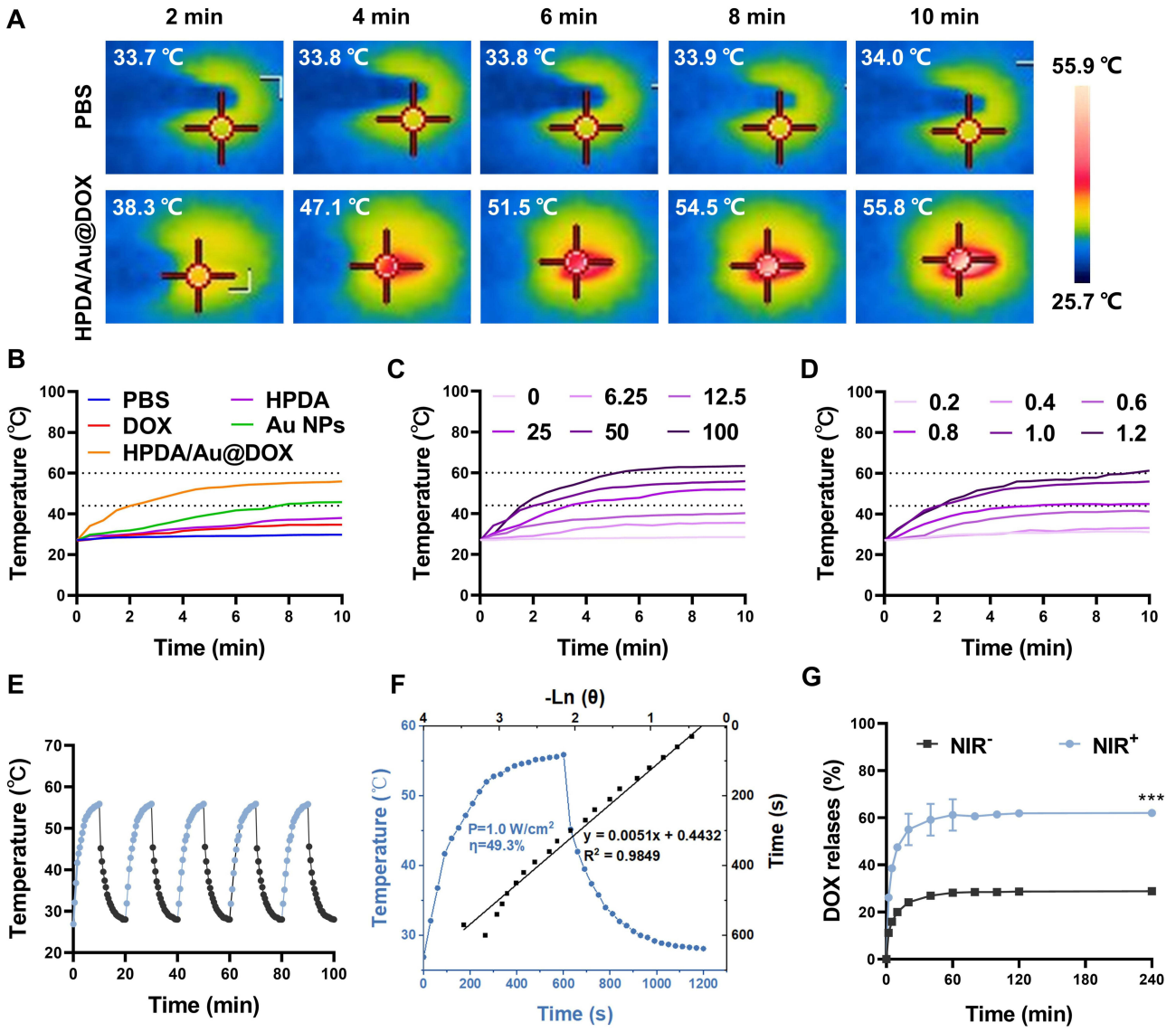

Figure 2 (**A**) Thermal imaging of PBS and 50 μg/mL HPDA/Au@DOX solution under 808 nm laser (1 W/cm^2) irradiation. (**B**) Heating curves of PBS, HPDA, DOX, Au nanoparticles (NPs), and 50 μg/mL HPDA/Au@DOX solution under 808 nm laser (1 W/cm^2) irradiation. (**C**) Heating curves of different concentrations (0, 6.25, 12.5, 25, 50, 100 μg/mL) of HPDA/Au@DOX solution under 808 nm laser (1 W/cm^2) irradiation. (**D**) Heating curves of 50 μg/mL HPDA/Au@DOX solution under different 808 nm laser power densities (0.2, 0.4, 0.6, 0.8, 1.0, 1.2 W/cm^2). (**E**) Photothermal stability of 50 μg/mL HPDA/Au@DOX solution under five on/off cycles of 808 nm laser (1 W/cm^2) irradiation. (**F**) Photothermal conversion efficiency of 50 μg/mL HPDA/Au@DOX solution under 808 nm laser (1 W/cm^2) irradiation. Heating-cooling curves (blue dashed line), t- -ln TETA plot (black straight line). (**G**) NIR laser-responsive release behavior of HPDA/Au@DOX (n=3). Two-way ANOVA with Sidak's multiple comparisons test was used for the statistical analysis of (**G**). ***$p < 0.001$.

microscopy. As shown in Figure 4, weak red fluorescence was observed only in the free DOX group, and the unirradiated HPDA/Au@DOX group also exhibited minimal red fluorescence. In contrast, the HPDA/Au@DOX+NIR group emitted strong fluorescence, indicating enhanced cellular uptake of HPDA/Au@DOX due to NIR laser irradiation. This is consistent with the previous study that demonstrated how photothermal effects can enhance nanoparticle uptake and drug release in cancer cells.[44]

Biocompatibility of HPDA/Au@DOX

Given the excellent photothermal properties and anti-tumor activity of HPDA/Au@DOX observed in vitro, it is necessary to further explore its feasibility and safety for in vivo applications. Firstly, the blood compatibility of HPDA/Au@DOX was evaluated through hemolysis assays. As shown in Figure 5A and 5B, except for the

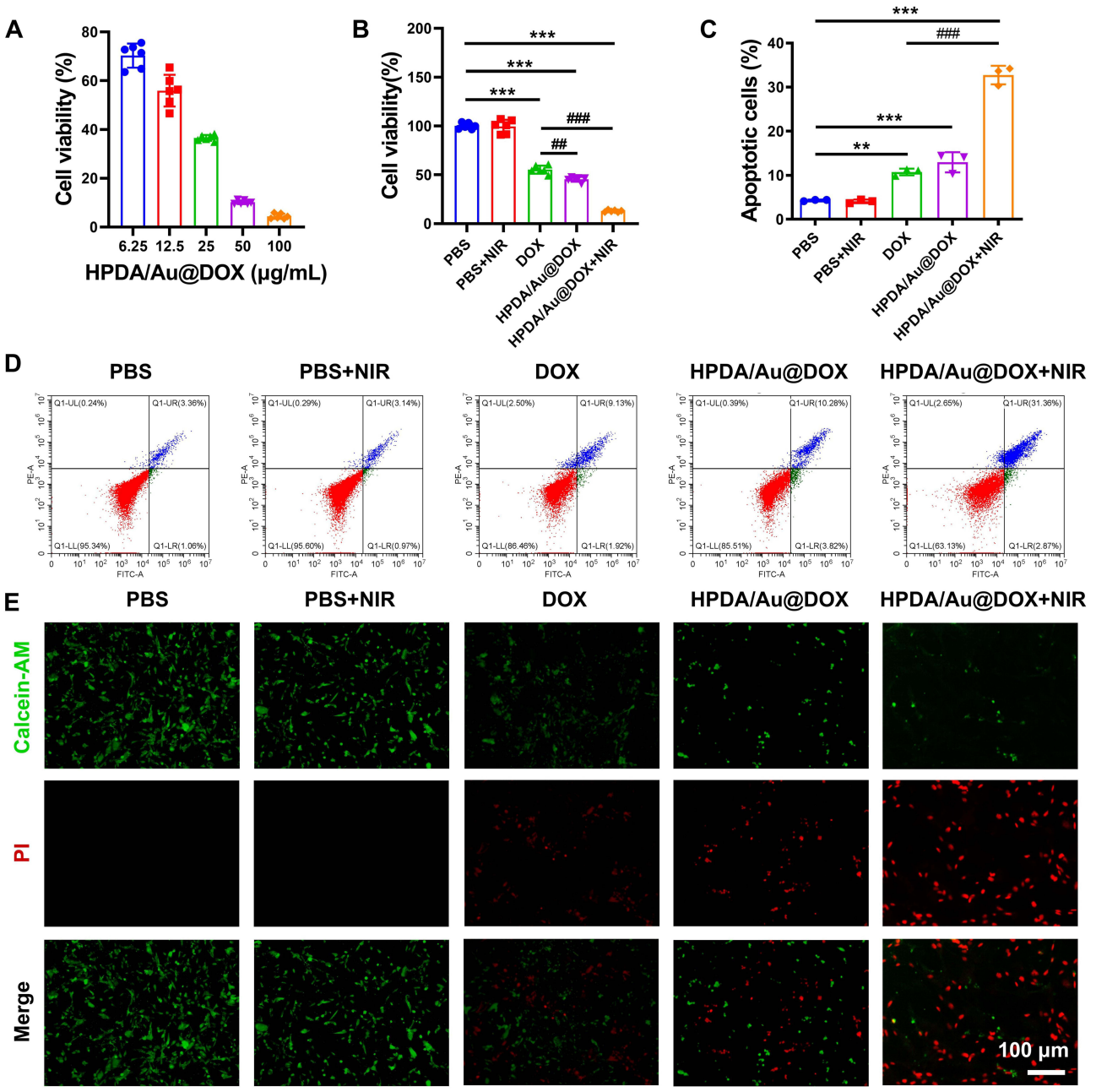

Figure 3 (**A**) The effect of different concentrations (6.25, 12.5, 25, 50, 100 μg/mL) of HPDA/Au@DOX solution on the viability of A549 cells under NIR laser irradiation (n=6). (**B**) The effect of different treatment groups (50 μg/mL for HPDA/Au@DOX) on the proliferation of A549 cells as detected by CCK-8 assay (n=6). (**C**) Quantification of apoptosis rates in A549 cells from different treatment groups (50 μg/mL for HPDA/Au@DOX; n=3). (**D**) The effect of different treatment groups on apoptosis of A549 cells as detected by flow cytometry. (**E**) Live/dead imaging of A549 cells from different treatment groups (n=3). The normality of the data was verified using the Shapiro–Wilk test. One-way ANOVA with Tukey's HSD test was used for statistical analysis of (**B** and **C**). $^{**}p < 0.01$, $^{***}p < 0.001$, $^{\#\#}p < 0.01$, $^{\#\#\#}p < 0.001$.

concentration of 200 μg/mL, the hemolysis rate of HPDA/Au@DOX at other concentrations did not exceed 5%, indicating good blood compatibility and no hemolysis, which is consistent with other studies on PDA-based metal nanomaterials.[45] Furthermore, the in vivo toxicity of anti-tumor drugs directly affects patient survival rates and treatment compliance.[46] Using PBS as a negative control, in vivo toxicity of was assessed by intratracheal injection of HPDA/Au@DOX into mice. HE staining results showed no significant pathological damage in the heart, liver, spleen, lungs, and kidneys of mice in the HPDA/Au@DOX group (Figure 5C). Additionally, further blood tests indicated no significant changes in ALT, AST, UREA, CRE, RBC, and PLT levels in mice of the

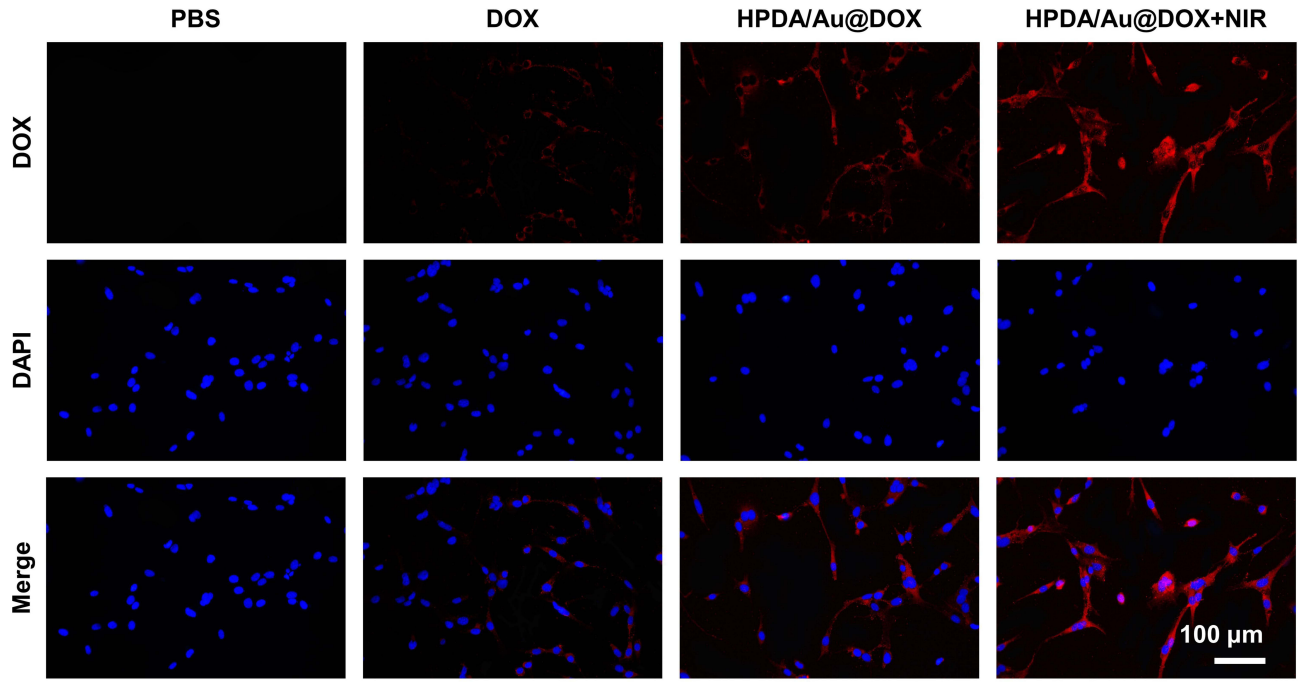

Figure 4 DOX uptake in A549 cells (n=3). DOX fluorescence was measured using an excitation wavelength of 480 nm and an emission wavelength of 590 nm.

HPDA/Au@DOX group within 15 days (Figure 5D–I), suggesting that HPDA/Au@DOX does not cause bone marrow suppression, liver toxicity, or kidney toxicity.

Anti-Metastatic Effect of HPDA/Au@DOX

Based on the excellent biocompatibility of this nanomaterial, we further explored their application in vivo. To investigate the anti-metastatic potential, we established an NSCLC lung metastasis model by injecting A549 cells into the tail veins of mice. The low accumulation of anticancer drugs in tumors and the severe systemic toxicity remain the main challenges to the clinical efficacy of drugs.[47] Pulmonary drug delivery strategies can rapidly and accurately deliver drugs to the lungs, increase drug concentration in tumors, reduce dosing frequency, and minimize systemic toxicity.[48] Initially, we investigated the biodistribution of intratracheally administered HPDA/Au@DOX in lung metastasis mice. As shown in Figure 6A, the fluorescence signal in the tumor area gradually increased with time, reaching a peak at 12 h and then decreasing. Therefore, we chose to perform NIR laser irradiation 12 h after intratracheal injection of HPDA/Au@DOX. In addition, ex vivo tissue imaging results (Figure 6B) showed that HPDA/Au@DOX was mainly distributed in lung tissue, with only a small amount in liver, spleen, and kidney tissues. These results indicate that pulmonary delivery achieved selective accumulation of HPDA/Au@DOX in lung tissue. After the completion of drug treatment in lung metastasis mice, with or without NIR laser irradiation, it was observed by the naked eye that there were more metastatic nodules in the ex vivo lung tissue injected with PBS (Figure 6C). Compared to the PBS group, mice given free DOX or HPDA/Au@DOX alone showed a reduction in surface metastatic foci in the lungs. Combining with 808 nm laser irradiation further enhanced the anti-metastatic efficacy of HPDA/Au@DOX, significantly reducing the surface metastatic foci in the lungs of mice. The metastatic lung nodules were confirmed by H&E staining (Figure 6D). Overall, these results suggest that HPDA/Au@DOX may play a functional role in regulating cancer metastasis.

In vivo Antitumor Effect of HPDA/Au@DOX

Finally, further elucidating the potential antitumor effect of HPDA/Au@DOX on NSCLC. As shown in Figure 7A, on the 10th day after subcutaneous transplantation of A549 cells in mice, drug administration and

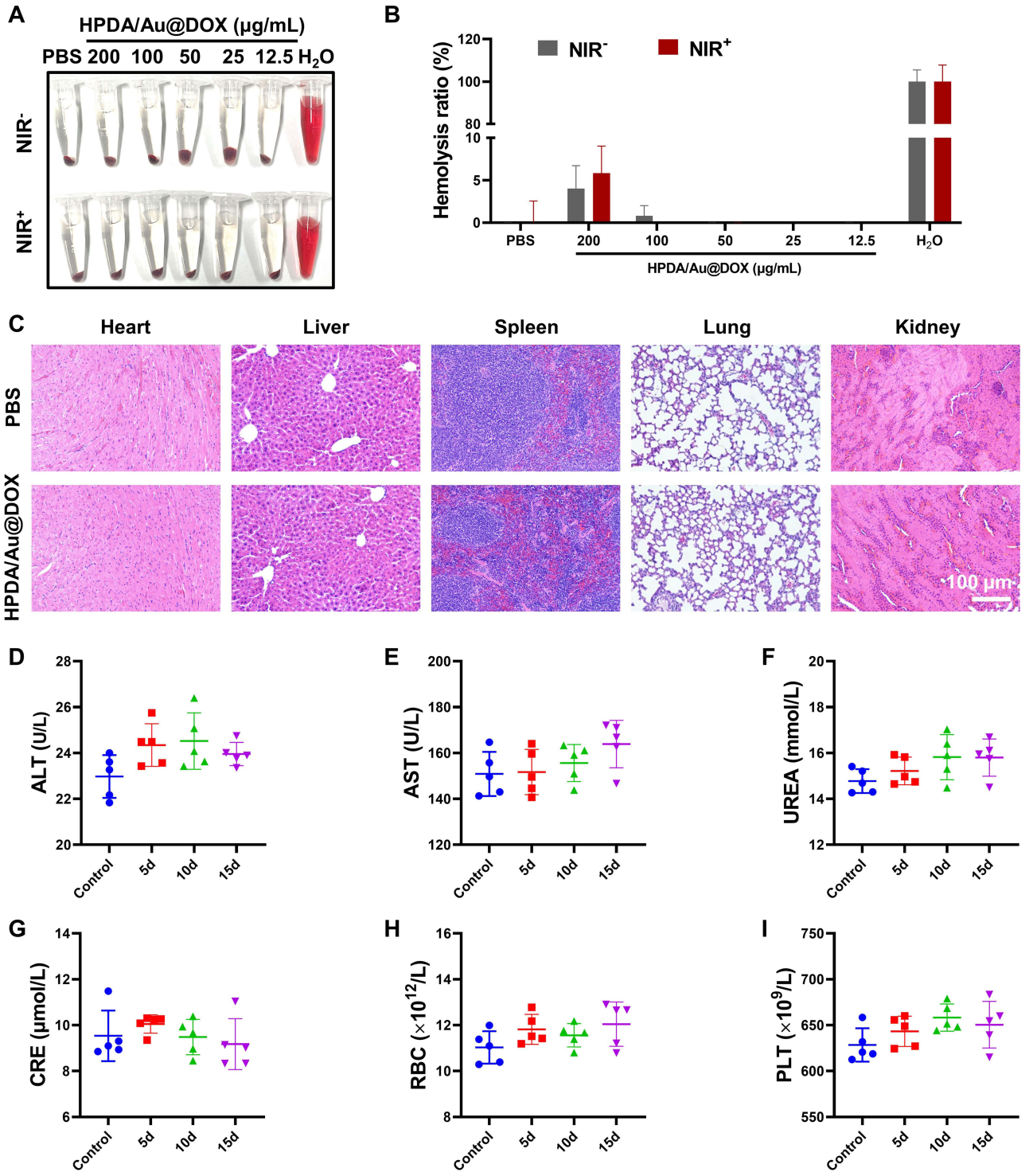

Figure 5 (**A** and **B**) Hemolysis test image (**A**) and hemolysis rate (**B**) (n=3). (**C**) HE staining of heart, liver, spleen, lungs, and kidneys (scale bar, 100 μm). (**D**–**I**) Changes in serum levels of ALT (**D**), AST (**E**), UREA (**F**), CRE (**G**), RBC (**H**), and PLT (**I**) within 15 days after injection of HPDA/Au@DOX (n=5). Repeated measures ANOVA was used for statistical analysis of (**D**–**F, H** and **I**), while Friedman test was used for statistical analysis of (**G**). The results showed no significant differences between groups.
Abbreviations: ALT, alanine aminotransferase; AST, aspartate aminotransferase; CRE, cyclization recombinase; RBC, red blood cell; PLT, platelet.

laser intervention began. Thermal imaging results revealed a significant increase in tumor temperature revealed a significant increase in tumor temperature from 35.6°C to 51.6°C after 10 minutes of laser irradiation in mice treated with HPDA/Au@DOX (Figure 7B and C). This high temperature not only induces thermal death of tumor cells but also aids in drug release, enabling chemo-thermal combined effects.[20,49] Throughout the treatment

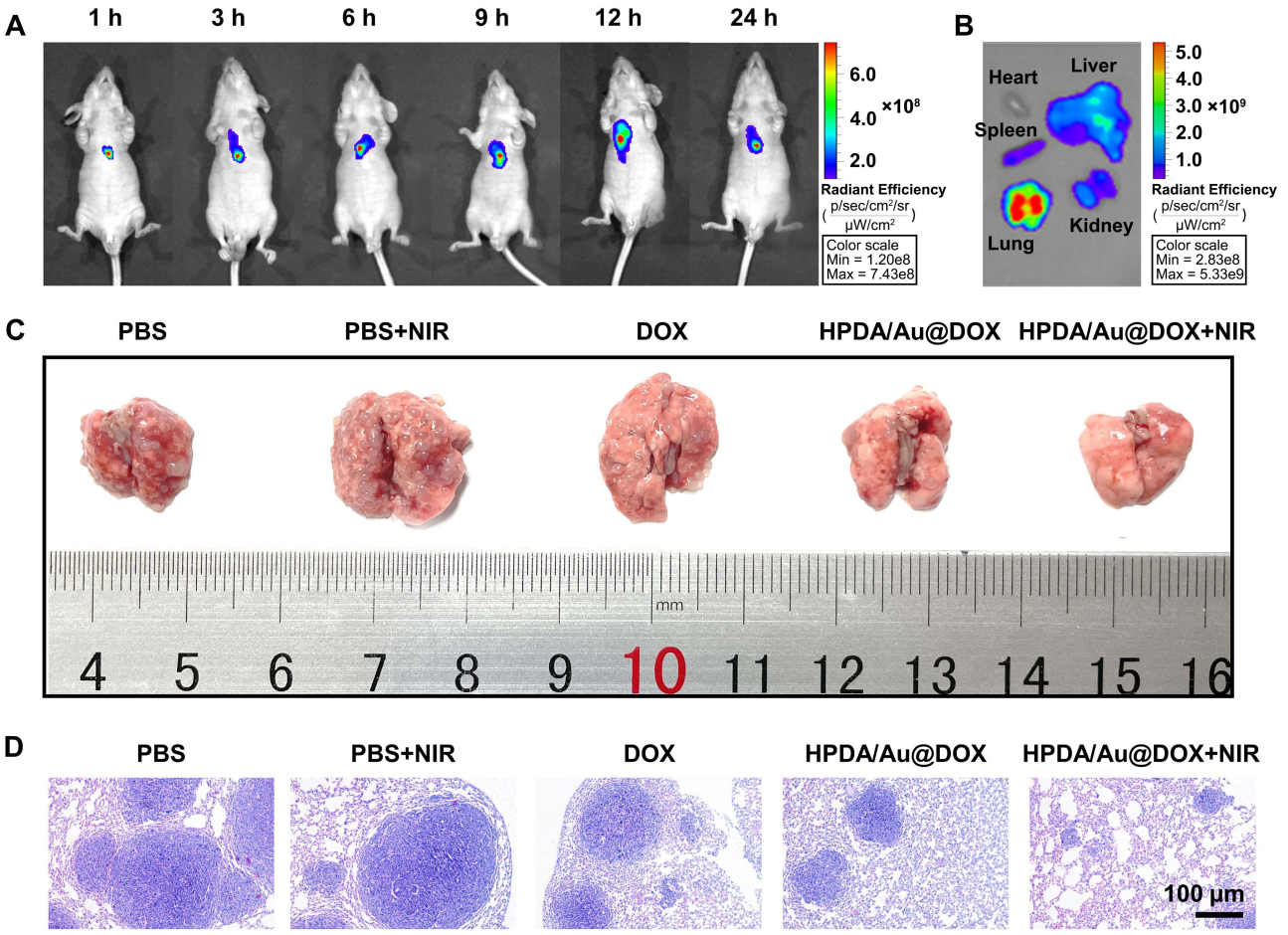

Figure 6 (**A**) In vivo fluorescence imaging for visualizing the biodistribution of HPDA/Au@DOX. (**B**) Ex vivo fluorescence imaging of major organs after in vivo imaging. Images were captured using a small animal in vivo imaging system (PerkinElmer, IVIS Spectrum). The colors in the images represent fluorescence intensity, with a gradient from purple to red indicating increasing fluorescence intensity. Stronger fluorescence corresponds to higher DOX accumulation, reflecting the greater accumulation of HPDA/Au@DOX at that location. (**C**) Representative images of lung metastatic nodules. (**D**) Representative H&E staining images of lung sections (scale bar, 100 μm) (n=5).

process, mouse body weight and tumor volume were measured and recorded every two days. The average body weight of each group of nude mice slowly increased over time without significant changes (Figure 7D), which laterally corroborated that HPDA/Au@DOX did not exhibit acute toxic side effects in vivo. As shown in Figure 7E–G, regardless of NIR laser irradiation stimulation, the tumor volume of nude mice injected with PBS increased substantially over time. The growth rate of tumor volume was slowed down in mice injected with free DOX or HPDA/Au@DOX alone, demonstrating a certain inhibitory effect on tumor growth. Under NIR light irradiation conditions, the tumor volume growth in the HPDA/Au@DOX+NIR group was significantly slower, indicating a much stronger antitumor effect compared to other treatment groups. After the treatment, the HPDA/Au@DOX+NIR group exhibited the smallest tumor volume and weight (Figure 7H). These results collectively indicate that HPDA/Au@DOX+NIR exhibits excellent photothermal performance and anticancer efficacy in vivo.

Conclusion

This study successfully prepared HPDA/Au@DOX via polydopamine chemistry combined with the sacrificial template method, exhibiting good physiological stability, excellent photothermal characteristics, satisfactory biocompatibility, and high drug loading capacity. Through intratracheal administration, HPDA/Au@DOX can passively target and efficiently deliver DOX to tumor sites and the lungs. Under NIR light stimulation, it achieves the combination of chemotherapy and photothermal therapy on tumor cells, providing a new strategy and reference for the treatment of lung cancer.

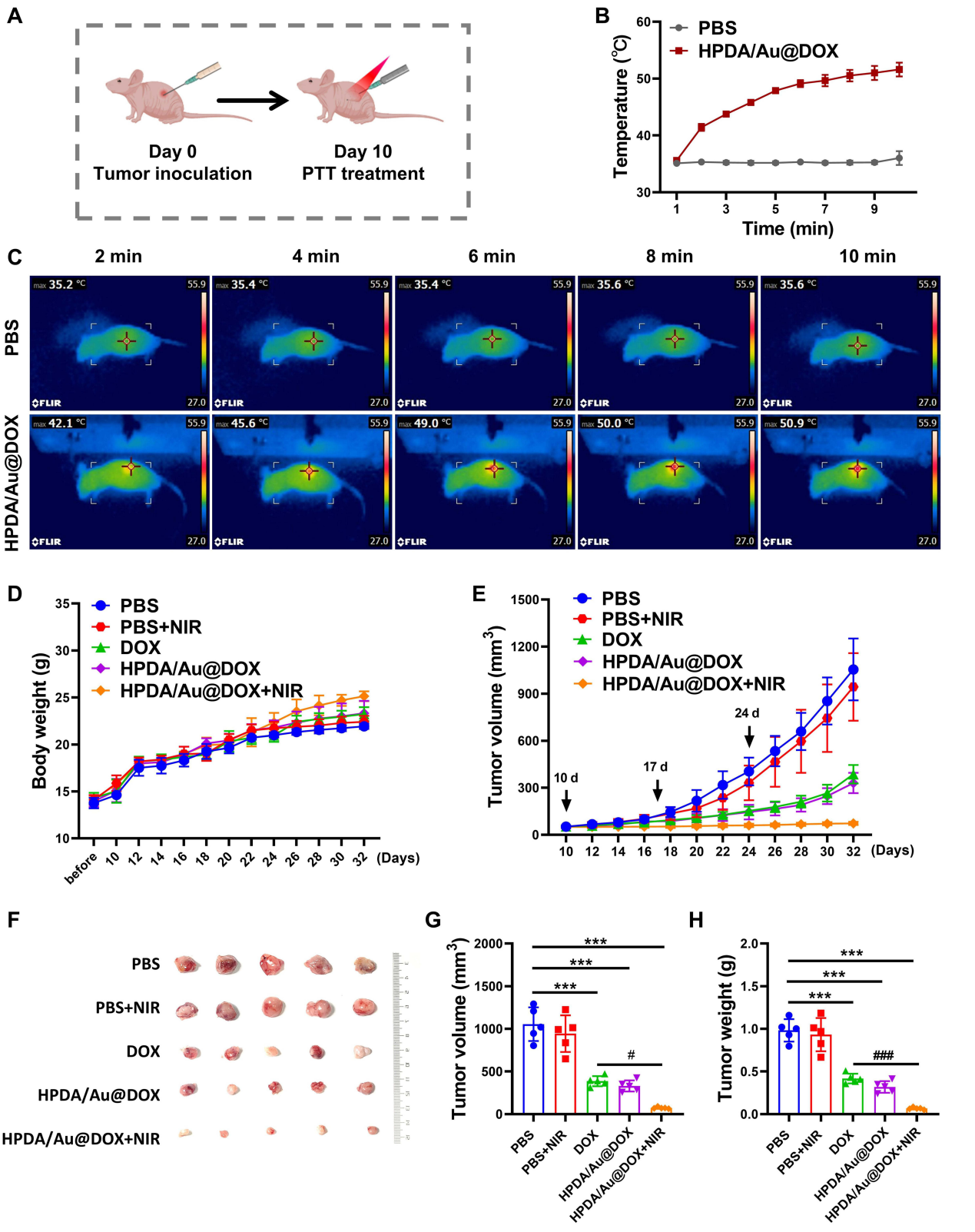

Figure 7 (**A**) Schematic representation of model construction and treatment in the A549 subcutaneous xenograft mice. (**B**) Temperature statistics of tumor photothermal imaging 12 hours after administration of PBS and HPDA/Au@DOX. (**C**) Representative infrared thermal images of tumors 12 hours after administration of PBS and HPDA/Au@DOX. (**D**) Changes in body weight of mice in each group during the treatment period. (**E**) Changes in tumor volume of mice in each group during the treatment period. (**F**) Images of dissected tumors from mice after the treatment. (**G**) Tumor volume statistics of each group after the treatment. (**H**) Tumor weight statistics of each group after the treatment (n=5). The normality of the data was verified using the Shapiro–Wilk test. One-way ANOVA with Tukey's HSD test was used for statistical analysis of (**G** and **H**). $^{***}p < 0.001$, $^{\#}p < 0.05$, $^{\#\#\#}p < 0.001$.

Data Sharing Statement

Data used and analyzed during the current study are available from the corresponding author on reasonable request.

Consent for Publication

All the authors consent for publication.

Funding

This study was supported by the Wenzhou Science and Technology Bureau Project (Grant No. 2022Y0370).

Disclosure

The authors report no conflicts of interest in this work.

References

1. Thai AA, Solomon BJ, Sequist LV, Gainor JF, Heist RS. Lung cancer. *Lancet*. 2021;398(10299):535–554. doi:10.1016/S0140-6736(21)00312-3
2. Wu C, Li M, Meng H, et al. Analysis of status and countermeasures of cancer incidence and mortality in China. *Sci China Life Sci*. 2019;62(5):640–647. doi:10.1007/s11427-018-9461-5
3. Sands J, Tammemagi MC, Couraud S, et al. Lung screening benefits and challenges: A review of the data and outline for implementation. *J Thorac Oncol*. 2021;16(1):37–53. doi:10.1016/j.jtho.2020.10.127
4. Chen P, Liu Y, Wen Y, Zhou C. Non-small cell lung cancer in China. *Cancer Commun* 2022;42(10):937–970. doi:10.1002/cac2.12359
5. Aix SP, Ciuleanu TE, Navarro A, et al. Combination lurbinectedin and doxorubicin versus physician's choice of chemotherapy in patients with relapsed small-cell lung cancer (ATLANTIS): A multicentre, randomised, open-label, Phase 3 trial. *Lancet Respir Med*. 2023;11(1):74–86. doi:10.1016/S2213-2600(22)00309-5
6. Ahn B-C, Kim HY, Lee GK, et al. Abstract 5539: Nivolumab after cyclophosphamide and doxorubicin induction therapy in previously treated advanced non-squamousl non-small cell lung cancer with PD-L1<10%. *Cancer Res*. 2022;82(12_Supplement):5539.
7. Paz-Ares L, Ciuleanu T, Navarro A, et al. PL02. 03 lurbinectedin/doxorubicin versus CAV or topotecan in relapsed SCLC patients: Phase III randomized ATLANTIS trial. *J Thorac Oncol*. 2021;16(10):S844–S845. doi:10.1016/j.jtho.2021.08.030
8. van der Zanden SY, Qiao X, Neefjes J. New insights into the activities and toxicities of the old anticancer drug doxorubicin. *FEBS J*. 2021;288(21):6095–6111. doi:10.1111/febs.15583
9. Dempke WCM, Zielinski R, Winkler C, Silberman S, Reuther S, Priebe W. Anthracycline-induced cardiotoxicity - are we about to clear this hurdle? *Eur J Cancer*. 2023;185:94–104. doi:10.1016/j.ejca.2023.02.019
10. Swain SM, Whaley FS, Ewer MS. Congestive heart failure in patients treated with doxorubicin: A retrospective analysis of three trials. *Cancer*. 2003;97(11):2869–2879. doi:10.1002/cncr.11407
11. Goncalves M, Mignani S, Rodrigues J, Tomas H. A glance over doxorubicin based-nanotherapeutics: From proof-of-concept studies to solutions in the market. *J Control Release*. 2020;317:347–374. doi:10.1016/j.jconrel.2019.11.016
12. Moradi Kashkooli F, Soltani M, Souri M. Controlled anti-cancer drug release through advanced nano-drug delivery systems: Static and dynamic targeting strategies. *J Control Release*. 2020;327:316–349. doi:10.1016/j.jconrel.2020.08.012
13. Manzari MT, Shamay Y, Kiguchi H, Rosen N, Scaltriti M, Heller DA. Targeted drug delivery strategies for precision medicines. *Nat Rev Mater*. 2021;6(4):351–370. doi:10.1038/s41578-020-00269-6
14. Yu H, Jin F, Liu D, et al. ROS-responsive nano-drug delivery system combining mitochondria-targeting ceria nanoparticles with atorvastatin for acute kidney injury. *Theranostics*. 2020;10(5):2342–2357. doi:10.7150/thno.40395
15. Li F, Qin Y, Lee J, et al. Stimuli-responsive nano-assemblies for remotely controlled drug delivery. *J Control Release*. 2020;322:566–592. doi:10.1016/j.jconrel.2020.03.051
16. Gannimani R, Walvekar P, Naidu VR, Aminabhavi TM, Govender T. Acetal containing polymers as pH-responsive nano-drug delivery systems. *J Control Release*. 2020;328:736–761. doi:10.1016/j.jconrel.2020.09.044
17. Cheng Z, Li M, Dey R, Chen Y. Nanomaterials for cancer therapy: current progress and perspectives. *J Hematol Oncol*. 2021;14(1):85. doi:10.1186/s13045-021-01096-0
18. Yi X, Duan QY, Wu FG. Low-temperature photothermal therapy: strategies and applications. *Res*. 2021;2021:9816594. doi:10.34133/2021/9816594
19. Yang K, Zhao S, Li B, Wang B, Lan M, Song X. Low temperature photothermal therapy: Advances and perspectives. *Coord Chem Rev*. 2022;454:214330. doi:10.1016/j.ccr.2021.214330
20. Li X, Lovell JF, Yoon J, Chen X. Clinical development and potential of photothermal and photodynamic therapies for cancer. *Nat Rev Clin Oncol*. 2020;17(11):657–674. doi:10.1038/s41571-020-0410-2
21. Wang S, Song Y, Cao K, et al. Photothermal therapy mediated by gold nanocages composed of anti-PDL1 and galunisertib for improved synergistic immunotherapy in colorectal cancer. *Acta Biomater*. 2021;134:621–632. doi:10.1016/j.actbio.2021.07.051
22. Sun P, Qu F, Zhang C, et al. NIR-II excitation phototheranostic platform for synergistic photothermal therapy/chemotherapy/chemodynamic therapy of breast cancer bone metastases. *Adv Sci*. 2022;9(33):e2204718. doi:10.1002/advs.202204718
23. Wang F, Li J, Chen C, Qi H, Huang K, Hu S. Preparation and synergistic chemo-photothermal therapy of redox-responsive carboxymethyl cellulose/chitosan complex nanoparticles. *Carbohydr Polym*. 2022;275:118714. doi:10.1016/j.carbpol.2021.118714
24. Gao G, Sun X, Liang G. Nanoagent-promoted mild-temperature photothermal therapy for cancer treatment. *Adv Funct Mater*. 2021;31(25):2100738. doi:10.1002/adfm.202100738

25. Mu Y, Sun Q, Li B, Wan X. Advances in the synthesis and applications of mussel-inspired polymers. *Polymer Rev*. 2023;63(1):1–39. doi:10.1080/15583724.2022.2041032
26. Saraf M, Prateek, Ranjan R, Balasubramaniam B, Thakur VK, Gupta RK. Polydopamine-enabled biomimetic surface engineering of materials: New insights and promising applications. *Adv Mater Interfaces*. 2023;11:2300670.
27. Wang W, Tang Z, Zhang Y, Wang Q, Liang Z, Zeng X. Mussel-inspired polydopamine: The bridge for targeting drug delivery system and synergistic cancer treatment. *Macromol Biosci*. 2020;20(10):e2000222. doi:10.1002/mabi.202000222
28. Zhuang H, Su H, Bi X, et al. Polydopamine nanocapsule: A theranostic agent for photoacoustic imaging and chemo-photothermal synergistic therapy. *ACS Biomater Sci Eng*. 2017;3(8):1799–1808. doi:10.1021/acsbiomaterials.7b00260
29. Tabish TA, Dey P, Mosca S, et al. Smart gold nanostructures for light mediated cancer theranostics: combining optical diagnostics with photothermal therapy. *Adv Sci*. 2020;7(15):1903441. doi:10.1002/advs.201903441
30. Chen Y, Xu C, Cheng Y, Cheng Q. Photostability enhancement of silica-coated gold nanostars for photoacoustic imaging guided photothermal therapy. *Photoacoustics*. 2021;23:100284. doi:10.1016/j.pacs.2021.100284
31. Xu C, Wang Y, Wang E, et al. Effective eradication of tumors by enhancing photoacoustic-imaging-guided combined photothermal therapy and ultrasonic therapy. *Adv Funct Mater*. 2021;31(10):2009314. doi:10.1002/adfm.202009314
32. Wei Q, Arami H, Santos HA, et al. Intraoperative assessment and photothermal ablation of the tumor margins using gold nanoparticles. *Adv Sci*. 2021;8(5):2002788. doi:10.1002/advs.202002788
33. Hajfathalian M, de Vries CR, Hsu JC, et al. Theranostic gold-in-gold cage nanoparticles enable photothermal ablation and photoacoustic imaging in biofilm-associated infection models. *J Clin Invest*. 2023;133(21). doi:10.1172/JCI168485.
34. Amina SJ, Guo B. A review on the synthesis and functionalization of gold nanoparticles as a drug delivery vehicle. *Int J Nanomed*. 2020;15:9823–9857. doi:10.2147/IJN.S279094
35. Shang B, Zhang X, Ji R, et al. Preparation of colloidal polydopamine/Au hollow spheres for enhanced ultrasound contrast imaging and photothermal therapy. *Mater Sci Eng C Mater Biol Appl*. 2020;106:110174. doi:10.1016/j.msec.2019.110174
36. Zhang G, Cheng W, Du L, Xu C, Li J. Synergy of hypoxia relief and heat shock protein inhibition for phototherapy enhancement. *J Nanobiotech*. 2021;19(1):9. doi:10.1186/s12951-020-00749-5
37. Shi Y, van der Meel R, Chen X, Lammers T. The EPR effect and beyond: Strategies to improve tumor targeting and cancer nanomedicine treatment efficacy. *Theranostics*. 2020;10(17):7921–7924. doi:10.7150/thno.49577
38. Safari Yazd H, Yang Y, Li L, et al. Precise deposition of polydopamine on cancer cell membrane as artificial receptor for targeted drug delivery. *iScience*. 2020;23(12):101750. doi:10.1016/j.isci.2020.101750
39. Ahmed A, Sarwar S, Hu Y, et al. Surface-modified polymeric nanoparticles for drug delivery to cancer cells. *Expert Opin Drug Deliv*. 2021;18(1):1–24. doi:10.1080/17425247.2020.1822321
40. Yu D, Wang Y, Chen J, et al. Co-delivery of NIR-II semiconducting polymer and pH-sensitive doxorubicin-conjugated prodrug for photothermal/chemotherapy. *Acta Biomater*. 2022;137:238–251. doi:10.1016/j.actbio.2021.10.009
41. Pu XQ, Ju XJ, Zhang L, et al. Novel multifunctional stimuli-responsive nanoparticles for synergetic chemo-photothermal therapy of tumors. *ACS Appl Mater Interfaces*. 2021;13(24):28802–28817. doi:10.1021/acsami.1c05330
42. Guan S, Liu X, Fu Y, et al. A biodegradable "Nano-donut" for magnetic resonance imaging and enhanced chemo/photothermal/chemodynamic therapy through responsive catalysis in tumor microenvironment. *J Colloid Interface Sci*. 2022;608:344–354. doi:10.1016/j.jcis.2021.09.186
43. Sabourian P, Yazdani G, Ashraf SS, et al. Effect of physico-chemical properties of nanoparticles on their intracellular uptake. *Int J Mol Sci*. 2020;21(21):8019. doi:10.3390/ijms21218019
44. Fan R, Chen C, Hou H, et al. Tumor acidity and near-infrared light responsive dual drug delivery polydopamine-based nanoparticles for chemo-photothermal therapy. *Adv Funct Mater*. 2021;31(18):2009733. doi:10.1002/adfm.202009733
45. Liu Y, Ma Q, Tang L, et al. A multifunctional hydrogel with mild photothermal antibacterial and antioxidant properties based on quercetin and dopamine-coated zinc oxide nanoparticles for healing bacteria-infected wound. *Chem Eng J*. 2024;497:154518. doi:10.1016/j.cej.2024.154518
46. Cespedes Feliciano EM, Chen WY, Lee V, et al. Body composition, adherence to anthracycline and taxane-based chemotherapy, and survival after nonmetastatic breast cancer. *JAMA Oncol*. 2020;6(2):264–270. doi:10.1001/jamaoncol.2019.4668
47. Sun D, Gao W, Hu H, Zhou S. Why 90% of clinical drug development fails and how to improve it? *Acta Pharm Sin B*. 2022;12(7):3049–3062. doi:10.1016/j.apsb.2022.02.002
48. Thakur AK, Chellappan DK, Dua K, Mehta M, Satija S, Singh I. Patented therapeutic drug delivery strategies for targeting pulmonary diseases. *Expert Opin Ther Pat*. 2020;30(5):375–387. doi:10.1080/13543776.2020.1741547
49. Usta DD, Celebi N, Soysal F, Saglam ASY, Yildiz N, Salimi K. Bio-inspired NIR responsive Au-pDA@ pDA sandwich nanostructures with excellent photo-thermal performance and stability. *Colloids SurfPhysicochem Eng Asp*. 2021;611:125758. doi:10.1016/j.colsurfa.2020.125758